Lecture Notes in Civil Engineering

Arvind Kumar Agnihotri
Krishna R. Reddy
Ajay Bansal *Editors*

Geoenvironmental Engineering

Proceedings of EGRWSE-23, Volume 1

Springer

Lecture Notes in Civil Engineering

Volume 508

Lecture Notes in Civil Engineering (LNCE) publishes the latest developments in Civil Engineering—quickly, informally and in top quality. Though original research reported in proceedings and post-proceedings represents the core of LNCE, edited volumes of exceptionally high quality and interest may also be considered for publication. Volumes published in LNCE embrace all aspects and subfields of, as well as new challenges in, Civil Engineering. Topics in the series include:

- Construction and Structural Mechanics
- Building Materials
- Concrete, Steel and Timber Structures
- Geotechnical Engineering
- Earthquake Engineering
- Coastal Engineering
- Ocean and Offshore Engineering; Ships and Floating Structures
- Hydraulics, Hydrology and Water Resources Engineering
- Environmental Engineering and Sustainability
- Structural Health and Monitoring
- Surveying and Geographical Information Systems
- Indoor Environments
- Transportation and Traffic
- Risk Analysis
- Safety and Security

To submit a proposal or request further information, please contact the appropriate Springer Editor:

– Pierpaolo Riva at pierpaolo.riva@springer.com (Europe and Americas);
– Swati Meherishi at swati.meherishi@springer.com (Asia—except China, Australia, and New Zealand);
– Wayne Hu at wayne.hu@springer.com (China).

All books in the series now indexed by Scopus and EI Compendex database!

Arvind Kumar Agnihotri · Krishna R. Reddy · Ajay Bansal
Editors

Geoenvironmental Engineering

Proceedings of EGRWSE-23, Volume 1

Springer

Editors
Arvind Kumar Agnihotri
Department of Civil Engineering
Dr. B. R. Ambedkar National Institute
of Technology
Jalandhar, Punjab, India

Ajay Bansal
Department of Chemical Engineering
Dr. B. R. Ambedkar National Institute
of Technology
Jalandhar, Punjab, India

Krishna R. Reddy
Department of Civil, Materials
and Environmental Engineering
University of Illinois
Chicago, IL, USA

ISSN 2366-2557 ISSN 2366-2565 (electronic)
Lecture Notes in Civil Engineering
ISBN 978-981-97-3822-9 ISBN 978-981-97-3823-6 (eBook)
https://doi.org/10.1007/978-981-97-3823-6

Preface

Geo-environmental engineering is a comprehensive field that acknowledges the complex environmental issues requiring the collective expertise of various traditional disciplines. The term "Geo-Environmental Engineering" encompasses the collaborative efforts of geotechnical engineers, environmental engineers, hydrogeologists, earth scientists, geochemists, water engineers, biologists, ecologists, and others. Their contributions play a vital role in environmental management, site characterization, environmental risk assessment, waste disposal, soil and groundwater remediation, habitat protection, and environmental rehabilitation. This book compiles a range of multidisciplinary articles, serving as a valuable resource for students, professionals, practitioners, and researchers.

Given the diverse nature of problems addressed in Geo-Environmental Engineering, effective solutions often demand the involvement of professionals with a variety of educational backgrounds and training. The diversity among these experts can, however, pose challenges to efficient technical collaboration. Therefore, professionals with a broad knowledge base across the disciplines associated with geo-environmental problems can facilitate the necessary interaction for successful project completion in a multidisciplinary context. Geo-environmental engineering is an emerging and dynamic field that presents numerous technical challenges and opportunities to address multidisciplinary issues, ensuring the protection of public health, the environment, and promoting sustainable development.

Currently, the global population exceeds 7.4 billion, with conservative projections by the United Nations estimating a population of 11.1 billion by 2100, with around 80% of this growth occurring in developing countries. The driving factors behind the development of environmental geotechnology include population growth and rising living standards. As the need for more land increases with population growth, previously deemed unsuitable soil deposits are now utilized for residential housing and construction projects. Meanwhile, rising living standards contribute to industrial growth, resulting in increased pollution of air, water, and land, as well as heightened urban refuse production.

To address these challenges associated with problematic soil deposits and adverse environmental conditions, conventional construction technology must necessarily

take a new direction. The current soil mechanics concepts and methods for analyzing soil behavior under diverse environmental conditions are being challenged by problematic soil deposits and ground pollution issues. Consequently, the environmental aspects of geotechnology have expanded, leading to the emergence of geo-environmental engineering.

Jalandhar, India — Arvind Kumar Agnihotri
Chicago, USA — Krishna R. Reddy
Jalandhar, India — Ajay Bansal

Contents

Influence of Adsorption at Air–Water Interfaces on PFAS Transport 1
Md Khorshed Alam and Arvin Farid

Dynamics of Methane Oxidation by Biochar-Amended Landfill Cover Soil: Long-Term Near-Field Scale Experiments 11
Gaurav Verma, Jyoti K. Chetri, and Krishna R. Reddy

Strength Improvement of Kaolin with Biopolymers 25
Tugba Eskisar and Ayberk Temurayak

Use of Stabilized Steel Slag in Pavements 33
Hrushikesh Namdev Kedar, Satyajit Patel, and Sandesh S. Shirol

Experimental Investigation for Stabilization of Expansive Soil by Using Waste Materials—Brick Dust and Eggshell Powder 43
Marjom Ete, Moni Mishra, Ravino Mekro, Lensar Jamir, Taniya Oniya, Jeelek Rigia, and Ajanta Kalita

Enhancing the Stability of Black Cotton Soil Through Reinforcement with Fly Ash and Bagasse Ash Mixtures: A Comprehensive Overview 55
Bishnu Kant Shukla, Gaurav Bharti, Jyothi Chandrakantha Nagavi, Parikshit Hurukadli, Aakash Gupta, and Pushpendra Kumar Sharma

Soil Stabilization Through Microbial Bioenzymes: A Comprehensive Review of Recent Developments in Eco-Friendly Approaches 75
Bishnu Kant Shukla, Ruchi Saraswat, Gaurav Bharti, Pushpendra Kumar Sharma, Devendra Singh, Prashant Kumar Srivastava, Prashant Yadav, and Sahil Mishra

Geotechnical Behavior of Soil–Fly Ash–Cement Mix as Liner Material in Irrigation Canal 97
Pranjal Barman and Kangana Sarma

Heavy Metals Influence on the Geotechnical Performance of Black Cotton Soil for Liner Application 107
N. Mahesh Babu and Anil Kumar Mishra

Review of Leachate Liner Model Enhancements and Problem Articulation of Engineered Landfill for the Development of Leachate Containment System 119
Rohit Maurya, Madhuri Kumari, and Sanjay Kumar Shukla

Comparison of Immobilization Efficiency of Two Plant-Based Biochar for Pb-Contaminated Soil 133
Bhoomi Kamdar and Chandresh Solanki

Sustainability Assessment of MICP for Ground Improvement 143
Meghna Sharma

Investigation of Volume Deformation Behavior of Bentonite with Colemanite Addition in the Presence of High Temperature 153
Yusuf Batuge, Sukran Gizem Alpaydin, and Yeliz Yukselen-Aksoy

Impact of Alternative Daily Cover Materials Derived from Waste on Leachate Quality and Waste Degradation in Bioreactor Landfills 161
V. Jaya and P. Latha

Evaluate the Environmental Impact of Fly Ash and Bio-enzyme Treated Black Cotton Soil to Mitigate the Leaching Problem 175
S. S. Kushwaha, D. Kishan, and N. Dindorkar

The Effect of Graphite, Brass and Copper Powders and Bronze Additives on the Thermal Conductivity of Bentonite 185
Feyza Toygar and Yeliz Yukselen-Aksoy

Microplastics Occurrence in Urban Water: Current Insights 191
Ayushi Chaudhary, Ashwani Kumar, Rahul Singh Thakur, and Amit Kumar

Unveiling Site Contamination: Comprehensive Investigation, Health Risk Assessment, and Management 203
G. L. Sivakumar Babu, B. Prathima, and Kalyani Kulkarni

Hydrogeological Study of Contamination of Soil and Water in the Vicinity of Municipal Dumping Ground: A Case Study 219
Maitrey Sankalp, Anshika Gondwal, Arvind Kumar Agnihotri, Ajaz Ahmad Mir, Mahesh Patel, and Rajwinder Singh

Investigating Role of $BiVO_4$ Nanoparticles in Degradation of Textile Dye in Effluent Water 237
Baneesh Patial, Ajay Bansal, Renu Gupta, and Susheel K. Mittal

Shear Strength and Volumetric Deformation Behavior of Fiberglass Added Sand–Bentonite Mixtures 247
Esra Güneri and Yeliz Yukselen-Aksoy

Uncertainty and Sensitivity Analysis of Environmental Impacts in Flexible Pavement Construction Using Alternate Industrial Waste 257
Anshumali Mishra, Sarat Kumar Das, and Krishna R. Reddy

Study of CO_2 Hydrate Formation in Saline Water for Oceanic CO_2 Sequestration 271
Milind Ghoderao, Yogendra Kumar, Rahul Sarkhel, Jitendra Sangwai, and Swati Patil

Estimation of Nitrate Concentration in Groundwater Source Using Zonal Nitrate Balance Method in Male Village of Western Maharashtra 281
Aditya Khebudkar and Milind Sohoni

About the Editors

Dr. Arvind Kumar Agnihotri is Professor in the Department of Civil Engineering at NIT Jalandhar. He completed his Ph.D. from IIT Roorkee, M.Tech. from NIT Kurukshetra and B.E. from Panjab University Chandigarh. He possesses a work experience of around 34 years in research, teaching, and academic administration, with several years spent holding key leadership positions. His areas of interest are geotechnical and geoenvironmental engineering, reinforced earth (geosynthetics and geofibers), ground improvement and soil-structure interaction. He has supervised 15 Ph.D. theses and 58 M.Tech. dissertations. He has 85 publications in international refereed journals and 60 publications in various national and international conferences/symposia. He has served Head of the Civil Engineering department, Dean Academics, Dean Planning and Development, and officiated as Campus Director at Dr. B. R. Ambedkar National Institute of Technology, Jalandhar. He has completed several sponsored projects, including World Bank projects. He is Fellow/Member of many professional organizations like ASCE, IGS, ISTE, ISSMGE and IRC. He has organized many national and international events successfully. He has edited 5 books, and he is Reviewer of many international journals.

Dr. Krishna R. Reddy is University Scholar, Distinguished Researcher, and Professor of Civil and Environmental Engineering and Director of both the Sustainable Engineering Research and Geotechnical and Geoenvironmental Engineering laboratories at the University of Illinois Chicago (UIC), USA. He received his Ph.D. in civil engineering from the Illinois Institute of Technology in Chicago. Prior to joining UIC, he worked for three years in consulting as Geotechnical/Geoenvironmental Engineer. His research expertise includes environmental remediation, waste containment, beneficial use of waste and recycled materials and sustainable and resilient engineering. Dr. Reddy has authored four books, 298 journal papers, 30 edited books and conference proceedings, 25 book chapters and 200 conference papers. His h-index is 73 with more than 18,000 citations. Because of his excellent contributions, Dr. Reddy received several awards, such as the Fulbright US Scholar Award, ASCE Wesley W. Horner Award, ASTM Hogentogler Award, UIC Distinguished Researcher Award, University of Illinois Scholar Award and the University

of Illinois Award for Excellence in Teaching. He is Fellow of the American Society of Civil Engineers.

Dr. Ajay Bansal is Professor of Chemical Engineering at Dr. B. R. Ambedkar National Institute of Technology, Jalandhar, India. He received his Ph.D. in Chemical Engineering from Panjab University, Chandigarh; M.Tech. from Indian Institute of Technology, New Delhi; and B.E. from Government Engineering College, Raipur (now NIT Raipur). He received the university gold medal for being first in his batch of B.E. at Pt. Ravishankar University, Raipur. He has served as Head of Chemical Engineering Department for two terms and was Associate Dean for Research and Consultancy at NIT Jalandhar. Dr. Bansal has more than 28 years of teaching, consulting and research experience within the fields of chemical and environmental engineering. His research expertise includes areas, such as nano-photocatalysis, advanced oxidation processes, waste water treatment, solid waste management, multiphase reactors, and rheologically complex fluids. He has supervised 8 Ph.D. dissertations, published 3 books, 3 book chapters, 45 journal papers and 65 conference papers. Dr. Bansal is on the editorial board and is Reviewer of many journals. He has been Active Member of various professional societies and is Fellow of Institution of Engineers (India) and Fellow of Indian Institute of Chemical Engineers (IIChE), Kolkata. Dr. Bansal has served twice as Vice-President of IIChE. He has been Chairman and Honorary Secretary of Doaba Regional Centre of IIChE as well.

Influence of Adsorption at Air–Water Interfaces on PFAS Transport

Md Khorshed Alam and Arvin Farid

Abstract The persistent organic pollutants known as perfluoroalkyl substances (PFAS) are pervasive, linger in the environment, and pose a health risk to humans. Assessing the risk and reducing the hazards associated with PFAS requires understanding the mechanisms and factors influencing PFAS transit in soil–water systems. Employing a 2D numerical model, this study investigates the effects of adsorption onto interfaces between air and water on the transport of PFAS in vadose and saturated zones. Our numerical simulations' results demonstrate that a higher air content in soil substantially impedes the transit of PFAS, thereby converting the PFAS phase that has adsorbed onto the interfaces between air–water into a long-term source of groundwater contamination. By adhering to air–water interfaces, PFAS retard their migration and become more stationary within the soil matrix. These results highlight how crucial it is to take air–water interfaces into consideration when predicting the demise and transport of PFAS in areas of contamination. The comprehensive outcomes of this study possess the potential to considerably augment remediation strategies and approaches to decision-making for PFAS-tainted regions.

Keywords PFAS · Air–water interface · Numerical model

1 Introduction

PFAS are widely utilized across various industrial and commercial sectors, including non-stick coatings, firefighting foams, and water-repellent fabrics, and as a result, large amounts of them are found in soil and water systems [1–3]. Because of their persistence and ability to bioaccumulate and biomagnify in the food chain, PFAS are a possible long-term threat to ecosystems and human health. Research on PFAS and their transportation has become critical because of their pervasiveness, durability, and associated health hazards. Understanding the factors affecting the transportation

M. Khorshed Alam (✉) · A. Farid
Boise State University, Boise, ID 83725-2060, USA
e-mail: mdkhorshedalam@u.boisestate.edu

A. K. Agnihotri et al. (eds.), *Geoenvironmental Engineering*, Lecture Notes in Civil Engineering 508, https://doi.org/10.1007/978-981-97-3823-6_1

and behavior of PFAS is therefore essential for risk evaluation and employing precise remedial procedures.

Numerous factors, including adsorption onto the solid phase, molecular diffusion, advective transport, and mechanical dispersion, are known to affect the fate and transport of PFAS in saturated soil [4, 5]. Research on PFAS transport behavior, however, is yet in its infancy, and there are still lots of questions to look into and address [6]. The understanding of PFAS transport within soil systems remains a topic of significant interest despite substantial studies in recent years [7–10], primarily because of the complex nature of these environments, characterized by the interaction of numerous physical, chemical, and biological factors. Further research must be done in order to understand the complex interactions and processes that occur at air–water interfaces in order to effectively address and mitigate the environmental effects caused by PFAS contamination.

In the current work, a specific two-dimensional (2D) problem is investigated to ascertain how various air content levels affect the transit of PFAS in the soil environment. This study used numerical simulations to provide a comprehensive understanding of the dynamic interactions between PFAS and the soil medium under different air saturation conditions.

2 Methodology

2.1 Transport of PFAS

Multiple processes play a role in the complex process of PFAS transfer in the soil environment. The transportation process of PFAS can be characterized by the following equation for a 2D problem involving advection, mechanical dispersion, molecular diffusion, and adsorption onto solids (i.e., soil particles), and air–water interfaces can be described as follows [11]:

$$\left.\frac{\partial(\theta C)}{\partial t}\right|_{\text{Diffusion}} = \frac{\partial}{\partial x}\left(\theta D_x \frac{\partial C}{\partial x}\right) + \frac{\partial}{\partial z}\left(\theta D_z \frac{\partial C}{\partial z}\right), \tag{1a}$$

$$\left.\frac{\partial(\theta C)}{\partial t}\right|_{\text{Advection}} = -\frac{\partial}{\partial t}(\theta v_x C) - \frac{\partial}{\partial z}(\theta v_z C), \tag{1b}$$

$$\left.\frac{\partial(\theta C)}{\partial t}\right|_{\text{Solid Adsorption}} = -\frac{\partial}{\partial t}(A_{\text{aw}} K_{\text{aw}} C), \tag{1c}$$

$$\left.\frac{\partial(\theta C)}{\partial t}\right|_{\text{Air-water Adsorption}} = -\rho_b \frac{\partial}{\partial t} K_f C^N. \tag{1d}$$

The summations will be

$$\frac{\partial(\theta C)}{\partial t} = \frac{\partial}{\partial x}\left(\theta D_x \frac{\partial C}{\partial x}\right) + \frac{\partial}{\partial z}\left(\theta D_z \frac{\partial C}{\partial z}\right) - \frac{\partial}{\partial x}(\theta v_x C) - \frac{\partial}{\partial z}(\theta v_z C) - \rho_b \frac{\partial}{\partial t} K_f C^N - \frac{\partial}{\partial t}(A_{\mathrm{aw}} K_{\mathrm{aw}} C), \tag{1e}$$

where θ is the volumetric water content ($\mathrm{cm}^3/\mathrm{cm}^3$); C is the aqueous concentration of PFAS ($\mu\mathrm{mol}/\mathrm{cm}^3$); ρ_b is the bulk density of the porous medium (g/cm^3); K_f and N are fitting coefficients obtained from experimental data to fit the Freundlich solid adsorption isotherm; A_{aw} stands for the air–water interfacial area ($\mathrm{cm}^2/\mathrm{cm}^3$); K_{aw} is the air–water interfacial adsorption coefficient ($\mathrm{cm}^3/\mathrm{cm}^2$); q is the Darcy flux (cm/s); v_x and v_z are components of $v = q/\theta$, , the interstitial pore-water velocity (cm/s); and D_x and D_z are components of diffusion coefficient, $\boldsymbol{D}$ (cm^2/s).

2.2 Numerical Modeling

To undertake numerical modeling of PFAS transport, the governing equation (Eq. 1) is discretized through the use of a finite-difference numerical method. For first-order time and space derivatives in this discretization process, forward differences are used, whereas central differences are used for higher-order derivatives in both the temporal and spatial domains. Given the horizontal grid spacing (Δx) and vertical grid spacing (Δz) at a specific time increment (Δt), the discretized form of Eq. (1) is written as follows:

$$\begin{aligned}
&C_{i,j}^{t^{k+1}}\left(\begin{array}{l}
\dfrac{F_{i,j}}{\Delta t} + \dfrac{A_{\mathrm{aw}\,i,j}K_{\mathrm{aw}\,i,j}}{\Delta t} + \dfrac{\theta_{i,j}v_{x\,i,j+1}}{\Delta x}\dfrac{v_{x\,i,j}\theta_{i,j+1}}{\Delta x} - 3\dfrac{v_{x\,i,j}\theta_{i,j}}{\Delta x} \\
\quad + \dfrac{\theta_{i,j}v_{z\,i+1,j}}{\Delta z} + \dfrac{v_{z\,i,j}\theta_{i+1,j}}{\Delta z} - 3\dfrac{v_{z\,i,j}\theta_{i,j}}{\Delta z} + \dfrac{\theta_{i,j}D_{x\,i,j+1} + \theta_{i,j+1}D_{x\,i,j}}{\Delta x^2} \\
\quad + \dfrac{\theta_{i,j}D_{z\,i+1,j} + \theta_{i+1,j}D_{z\,i,j}}{\Delta z^2} + \dfrac{\theta_{i,j}}{\Delta t} + \dfrac{\theta_{\mathrm{i,j}}^{t^{k+1}} - \theta_{\mathrm{i,j}}^{t^k}}{2\Delta t}
\end{array}\right) \\
&- C_{i,j+1}^{t^{k+1}}\left(-\frac{\theta_{i,j}v_{x\,i,j}}{\Delta x} + \frac{\theta_{i,j}D_{x\,i,j+1} - \theta_{i,j}D_{x\,i,j}}{\Delta x^2} + \frac{\theta_{i,j+1}D_{x\,i,j}}{\Delta x^2}\right) \\
&- C_{i+1,j}^{t^{k+1}+1}\left(-\frac{\theta_{i,j}v_{z\,i,j}}{\Delta z} + \frac{\theta_{i+1,j}D_{z\,i,j}}{\Delta z^2} + \frac{\theta_{i,j}D_{z\,i+1,j} - \theta_{i,j}D_{z\,i,j}}{\Delta z^2}\right) - C_{i,j-1}^{t^{k+1}}\left(\frac{\theta_{i,j}D_{x\,i,j}}{\Delta x^2}\right) \\
&- C_{i-1,j}^{t^{k+1}}\left(\frac{\theta_{i,j}D_{z\,i,j}}{\Delta z^2}\right) = C_{\mathrm{i,j}}^{t^k}\left(\frac{F_{i,j}}{\Delta t} + \frac{A_{aw\,i,j}K_{aw\,i,j}}{\Delta t} + \frac{\theta_{i,j}}{\Delta t} - \frac{\theta_{\mathrm{i,j}}^{t^{k+1}} - \theta_{\mathrm{i,j}}^{t^k}}{2\Delta t}\right),
\end{aligned} \tag{2}$$

where $F = \rho_b \frac{\partial}{\partial t} K_f C^N$, $\theta_{i,j} = \frac{\theta_{i,j}^{t^{k+1}} + \theta_{i,j}^{t^k}}{2}$, $A_{\mathrm{aw}\,i,j} = \frac{A_{\mathrm{aw}\,i,j}^{t^{k+1}} + A_{\mathrm{aw}\,i,j}^{t^k}}{2}$, and $D_{i,j} = \frac{D_{i,j}^{t^{k+1}} + D_{i,j}^{t^k}}{2}$.

For each node, the aqueous concentration, denoted as C, on the left-hand side of Eq. (1e) is expressed as the weighted average of the values $C_{i,j}^{t^{k+1}}$ and $C_{i,j}^{t^k}$, where $C_{i,j}^{t^k}$ denotes the concentration of PFAS at Node (i, j) at time steps t^k and t^{k+1}. Moreover,

F and K_{aw} are nonlinear functions of C, and their updates are carried out using a modified successive iteration scheme [12]. In essence, the procedure start with an initial value of $C_{i,j}^{t^k}$ and $S_{\text{w}\,i,j}^{t^k}$ (degree of saturation), $F_{i,j}^{t^k}$ and $K_{\text{aw}\,i,j}^{t^k}$ are computed using the formula provided in [4] to initiate a time step to determine $C_{i,j}^{t^{k+1}}$, and prior to advancing to the subsequent time step, a modified successive iteration scheme is used to update the values of $F_{i,j}^{t^{k+1}}$ and $K_{\text{aw}\,i,j}^{t^{k+1}}$, until convergence to the optimal $F_{i,j}^{t^{k+1}}$ and $K_{\text{aw}\,i,j}^{t^{k+1}}$. By doing so, the linear equation system described in Eq. (1) can be solved while maintaining Eq. (2)'s linearity. Utilizing the mean values of F and K_{aw} at time t^{k+1} and t^k, $C_{i,j}^{t^{k+2}}$ is computed at the following time step, and another modified successive iteration is performed until the best $F_{i,j}^{t^{k+2}}$, and $K_{\text{aw}\,i,j}^{t^{k+2}}$ is obtained. This procedure will be continued until the final step has been accomplished.

2.3 Problem Formulation and Parameters

The schematic of the model simulating a PFAS spill on the ground surface, where PFAS diffuses through the vadose zone and enters the groundwater, is shown in Fig. 1. The saturated zone beneath the vadose zone is not simulated in this instance. Two different types of boundary conditions are used to simulate this.

In order to maintain a constant concentration and comply with Neumann boundary conditions, the numerical simulation includes the top boundary node and the entire bottom boundary as inlet and outlet boundaries, respectively. The Dirichlet boundary conditions are applied to the other boundaries, which are presented as impermeable boundaries. Given the consistent inflow of freshwater at the outlet and the stable supply of PFAS concentrations at the inlet, it can be claimed that there is no PFAS accumulation at the outlet at the bottom boundary. As a result of the outlet's plentiful freshwater supply, PFAS may be flushed out continuously rather than accumulating in the system. The developed code is capable of permitting PFAS concentrations on the bottom boundary to rise. It is assumed that the soil contains no PFAS contaminants

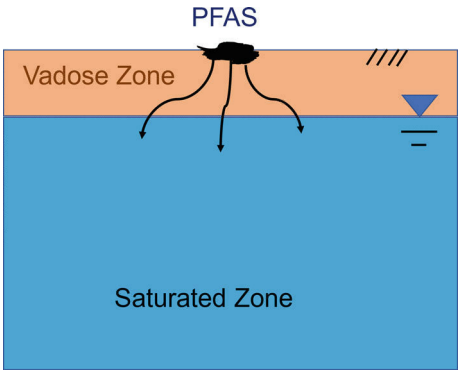

Fig. 1 Schematic of model layout for combinations involving a midpoint inlet on the top boundary and bottom boundary as outlet

Table 1 A list of variables and their corresponding values that are utilized for simulating Acusand soil

Parameter	Value	Unit
ρ_b	1.65	g/cm^3
K_f	0.055	(μmol/g)/(μmol/cm^3)^N
N	0.85	–
σ	71	dyne/cm
R	8.314	J/K/mol
T	293.15	K
a	0.004	μmol/cm^3
b	0.017	–
x_2	548.54	–
x_1	−1182.5	–
x_0	633.96	–

at the beginning. Therefore, none of the mesh grid's nodes had any concentration of PFAS. Following that, PFAS is first supplied at the inlet at a concentration of 12 μmol/cm^3. With the assumption of a constant PFAS supply at the inlet and a build-up of PFAS concentration at the outlets leading to breakthrough concentration, we were able to simulate PFAS transport using Neumann boundary conditions.

The Accusand soil type is taken into account for this study, and the following presumptions are taken into account in all scenarios for the simulations of PFAS transport: (i) the initial soil PFAS concentration is $C = 0$ μmol/cm^3; (ii) all other soil boundaries are impermeable, with the exception of the inlet at the top boundary and the bottom boundary outlet; (iii) PFAS concentration at the inlet is $C_1 = 12$ μmol/cm^3 and at the outlets is $C_2 = 0$ μmol/cm^3, throughout the periods of time; (iv) temporal increment is $\Delta t = 5$ seconds; (v) the vadose zone's size: length (in horizontal direction) $L = 2.1$ m and thickness (in vertical direction) $H = 2$ m; (vi) $D_x = 5.5 \times 10^{-3}$ m^2/s and $D_z = 1.5 \times 10^{-3}$ m^2/s ($D_{xz} = 0$ m^2/s) are components of the diffusion coefficient $\boldsymbol{D}$; (vii) soil porosity $n = 0.00294$; (viii) grid size of discretized soil sample is 26×14 (i.e., $dx = L/N - 1$ and $dz = T/M - 1$)(ix) there is unsaturated downward flow of water where velocity components $v_x = 0$ cm/s, $v_z = 1 \times 10^{-4}$ cm/s.

Furthermore, other essential parameters and data the necessary data and parameters were gathered from a study conducted by Guo et al. [4] presented in Table 1.

3 Simulation Results and Discussion

In order to investigate how air–water interfaces affect the transportation of PFAS, several scenarios were numerically simulated using the data from the preceding section. The results are displayed as temporal snapshots that illustrate the spatial

distribution of PFAS concentration at a time of 30,000 s. In addition, the temporal evolution of aqueous concentration at a specific point (a node at the center of the grid designated as a "Midpoint") is depicted.

3.1 Numerical Simulations

To investigate the impact of adsorption onto solid-phase interfaces on PFAS for various degrees of air content and water saturation, three scenarios have been simulated for: (i) Scenario 1—fully water saturated, i.e., $S_{\text{water}} = 1$ and $A_{\text{air}} = 0$; (ii) Scenario 2—partially water saturated with $S_{\text{water}} = 0.55$ and $A_{\text{air}} = 0.45$ and (iii) Scenario 3—partially water saturated with $S_{\text{water}} = 0.1$ and $A_{\text{air}} = 0.9$. Snapshots of the spatial distribution of PFAS' aqueous concentration at 30,000 s and the temporal profile of PFAS transportation at midpoint are presented below.

(i) **Scenario 1 ($A_{\text{air}} = 0$, $S_{\text{water}} = 1$)**

See Fig. 2.

(ii) **Scenario 2 ($A_{\text{air}} = 0.45$, $S_{\text{water}} = 0.55$)**

See Fig. 3.

(iii) **Scenario 3 ($A_{\text{air}} = 0.9$, $S_{\text{water}} = 0.1$)**

See Fig. 4.

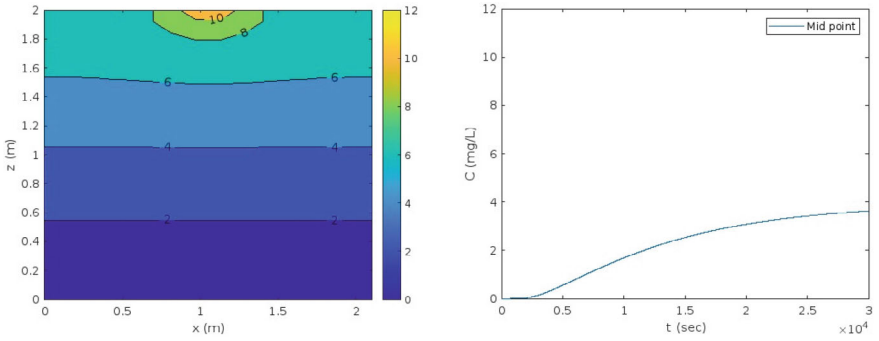

Fig. 2 PFAS transport under the influence of a steady inflow at the top boundary inlet and an outflow exposed to abundant freshwater at the bottom boundary encompasses: **a** spatial distribution of PFAS concentration at $t = 30{,}000$ s; **b** temporal profile of PFAS transportation at the midpoint node, considering the parameters, $A_{\text{air}} = 0$, and $S_{\text{water}} = 1$

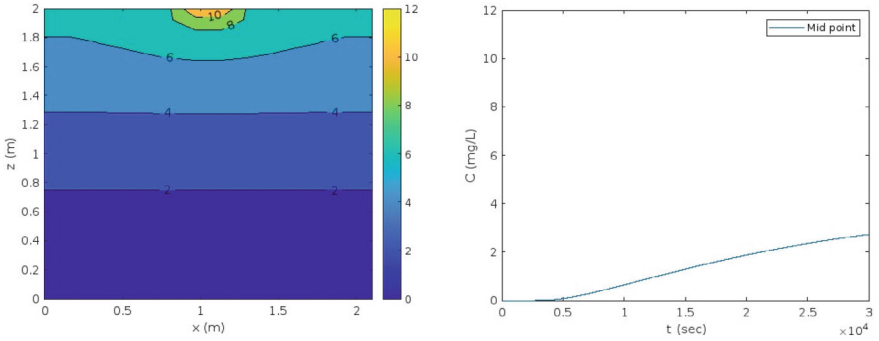

Fig. 3 PFAS transport under the influence of a steady inflow at the top boundary inlet and an outflow exposed to abundant freshwater at the bottom boundary encompasses: **a** spatial distribution of PFAS concentration at $t = 30{,}000$ s; **b** temporal profile of PFAS transportation at the midpoint node, considering the parameters $A_{\text{air}} = 0.45$, and $S_{\text{water}} = 0.55$

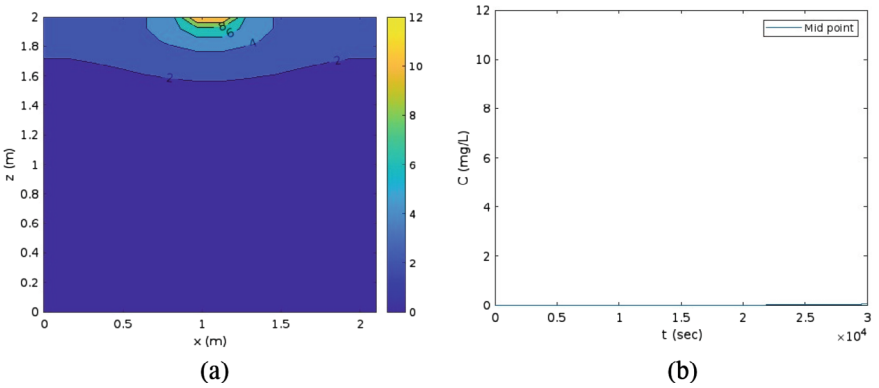

Fig. 4 PFAS transport under the influence of a steady inflow at the top boundary inlet and an outflow exposed to abundant freshwater at the bottom boundary encompasses: **a** spatial distribution of PFAS concentration at $t = 30{,}000$ s; **b** temporal profile of PFAS transportation at the midpoint node, considering the parameters $A_{\text{air}} = 0.9$, and $S_{\text{water}} = 1$

3.2 Discussion

The findings of the simulations outlined above exhibit how the air–water interface affects the spatial and temporal distribution of PFAS. In accordance with expectations, Fig. 2 shows that when the soil is completely water-saturated, the absence of air fosters rapid PFAS transport. As displayed in Fig. 3, the introduction of air to initially saturated soil hinders the transport of PFAS. Figure 4 then shows that a larger level of retardation happens when the soil becomes primarily air saturated. The PFAS transportation time history figures at the midpoint node also illustrate a

similar lag as the concentration of PFAS changes over a particular time frame. These temporal patterns highlight the critical role of adsorption and air in the soil matrix as key elements affecting the rates of PFAS transportation.

4 Conclusion

In the present study, in order to determine how PFAS adsorption onto interfaces between air and water affects the transport of PFAS, a 2D PFAS transport problem is numerically simulated. According to simulation results, adsorption onto air–water is one of the most important elements influencing the transport of PFAS in the soil environment and can have a substantial impact on its transport rates. As expected, PFAS movement is further hindered by the addition of more air to the saturated soil. The numerical model used in the present investigation offers a quantitative framework for thoroughly examining the impact on parameters like air–water interfaces and their individual contributions to PFAS transport, which could assist us in greater comprehending and foreseeing how PFAS will interact in the soil environment. The utilized numerical model, however, is based on a number of hypotheses and parametrizations that could result in ambiguities or flaws under realistic circumstances. This underscores the need for further study, including more precise and comprehensive 3D models, in order to improve the reliability as well as the practicality of the conclusions made in this work.

References

1. ITRC WI (2020) Per–and polyfluoroalkyl substances (PFAS)
2. List OGP (2018) Toward a new comprehensive global database of per-and polyfluoroalkyl substances (PFASs)
3. Buck RC et al (2011) Perfluoroalkyl and polyfluoroalkyl substances in the environment: terminology, classification, and origins. Integr Environ Assess Manage 7(4):513–541
4. Guo B, Zeng J, Brusseau ML (2020) A mathematical model for the release, transport, and retention of per-and polyfluoroalkyl substances (PFAS) in the vadose zone. Water Resour Res 56(2):e2019WR026667
5. Iradukunda P, Farid A (2022): Multiphysics numerical modeling of transient transport of PFAS, pp 149–158
6. Garg S, Wang J, Kumar P, Mishra V, Arafat H, Sharma RS, Dumée LF (2021) Remediation of water from per-/poly-fluoroalkyl substances (PFAS)–Challenges and perspectives. J Environ Chem Eng 9(4):105784
7. Brusseau ML (2023) Determining air-water interfacial areas for the retention and transport of Pfas and other interfacially active solutes in unsaturated porous media. Sci Total Environ 884:163730
8. Brusseau ML (2019) Estimating the relative magnitudes of adsorption to solid-water and air/oil-water interfaces for per-and poly-fluoroalkyl substances. Environ pollut 254:113102
9. Kim H, Annable MD, Rao PSC (1988) Influence of air–water interfacial adsorption and gas-phase partitioning on the transport of organic chemicals in unsaturated porous media. Environ Sci Technol 32(9):1253–1259

10. Lyu X, Xiao F, Shen C, Chen J, Park CM, Sun Y, Wang D et al (2022) Per-and polyfluoroalkyl substances (PFAS) in subsurface environments: occurrence, fate, transport, and research prospect. Rev Geophys 60(3):e2021RG000765
11. Zeng J, Guo B (2021) Multidimensional simulation of PFAS transport and leaching in the vadose zone: impact of surfactant-induced flow and subsurface heterogeneities. Adv Water Resour 155:104015
12. Jordan ED Jr (1981) A modified Crank-Nicolson method. Master Thesis, Virginian Commonwealth University

Dynamics of Methane Oxidation by Biochar-Amended Landfill Cover Soil: Long-Term Near-Field Scale Experiments

Gaurav Verma, Jyoti K. Chetri, and Krishna R. Reddy

Abstract The rising levels of methane (CH_4) in the atmosphere, driven by the combination of a growing population and higher energy/resource usage, have sparked worries about its contribution to climate change. Municipal solid waste (MSW) landfills are major contributors to global CH_4 emissions. Recent studies have highlighted the potential of biochar amendment in landfill cover soil to enhance microbial CH_4 oxidation. However, landfills also release carbon dioxide (CO_2), hydrogen sulfide (H_2S), and other gases that require mitigation. To address these concerns, a biogeochemical cover (BGCC) incorporating biochar-amended soil (BAS) and basic oxygen furnace (BOF) steel slag was developed earlier to concurrently remove CH_4, CO_2, and H_2S. Laboratory experiments demonstrated significant potential for CH_4, CO_2, and H_2S removal under simulated landfill cover conditions. However, the effectiveness of this cover in the field remains unexplored. To address this, a near-field scale tank setup of BGCC was established in the laboratory. The BGCC profile comprised of three-layers: a lower layer of 10% (w/w) BAS (45 cm), a middle layer of BOF slag (30 cm), and an upper topsoil vegetative soil layer (15 cm). Synthetic landfill gas was flushed through the tank in five phases with varying flow rates and composition. The scope of this paper is to present the CH_4 oxidation occurring within the BAS layer. Gas monitoring was performed within the biocover layer over time. CH_4 oxidation and physico-chemical properties were assessed at the same depth of gas concentrations monitoring but different spatial locations within the biocover layer. Results showed that Phase 2, with a 50% CH_4 and 50% CO_2 composition at a flux rate of 23.9 g CH_4 m^{-2} day^{-1}, achieved the maximum CH_4 reduction. Conversely, Phase 4 exhibited the lowest reduction due to a high influx rate nearly twice that of Phase 2. The BAS demonstrated CH_4 oxidation rates ranging from 227.5 to 333.7 μg CH_4 g^{-1} day^{-1} spatially at a depth of 50 cm below the ground (bgs) , highlighting its significant potential for CH_4 conversion into CO_2.

Keywords Methane oxidation · Biochar · Landfill cover · Landfill gas · Climate mitigation

G. Verma (✉) · J. K. Chetri · K. R. Reddy
University of Illinois Chicago, Chicago, IL 60607, USA
e-mail: gverma5@uic.edu

A. K. Agnihotri et al. (eds.), *Geoenvironmental Engineering*, Lecture Notes in Civil Engineering 508, https://doi.org/10.1007/978-981-97-3823-6_2

1 Introduction

The rapid increase in greenhouse gas emissions resulting from population growth and intensified energy/resource consumption has led to significant concern regarding the escalating levels of methane (CH_4), a potent greenhouse gas that contributes significantly to climate change. Among the various greenhouse gases, CH_4 has garnered significant attention due to its remarkably high global warming potential (GWP), which is approximately 27–30 times more than that of carbon dioxide (CO_2) [1]. While methane's atmospheric lifetime is relatively short, lasting approximately a decade, it is considerably lower than CO_2, which can persist for thousands of years. However, CH_4, with its exceptionally high energy adsorbing capacity compared to CO_2, results in a high GWP [1], posing a substantial risk to the environment and necessitating immediate attention.

Despite being widely considered as an unsustainable waste management method, landfilling of waste continues to be the primary approach adopted by many countries, including the USA. The municipal solid waste (MSW) disposed of in landfills underwent anaerobic decomposition, leading to the production of landfill gas (LFG), mainly consisting of CH_4 and CO_2, along with small quantities of hydrogen sulfide (H_2S) and other non-methane organic compounds. MSW landfills are reported to be the third largest source of CH_4 emissions in the USA, contributing 14.3% of total emissions in 2021 [2].

Landfill covers are constructed at the landfills to prevent the LFG emissions from escaping into the atmosphere. These cover soils naturally harbor CH_4-oxidizing microorganisms, due to continuous exposure of CH_4 produced from decomposition of MSW waste. In the presence of oxygen (O_2), these microorganisms effectively convert CH_4 into CO_2 through oxidation [3]. However, these soil covers do not fully capture all LFG, resulting in the release of a portion of (LFG) emissions into the atmosphere as fugitive emissions [4]. Gas collection wells are installed to capture the LFG; however, due to the limited radius of influence associated with gas collection wells, their effectiveness in mitigating landfill CH_4 emissions has been proven to be inadequate [4, 5].

Recent attempts have been directed toward improving the ability of landfill cover soils to oxidize CH_4 by incorporating different organic enhancements such as compost [6], sewage sludge [7], and biochar [8]. Among these amendments, biochar, a carbonaceous solid produced from biomass pyrolysis or gasification, has demonstrated potential as a suitable option for improving microbial CH_4 oxidation in landfill soil cover [8–10]. Biochar presents notable advantages compared to alternative organic amendments due to its distinctive characteristics, including its resistance to decomposition, capability to retain moisture, presence of micro-sized pores, specific surface area, and capacity to adsorb gases. In contrast, other amendments like compost and sewage sludge may undergo self-degradation over time, leading to reduction in CH_4 removal efficiency of biocover.

In addition to CH_4, LFG contains CO_2, small quantities of hydrogen sulfide (H_2S), and other gases. CO_2 is not solely produced from MSW but also results from the

oxidation of CH_4, thereby contributing to an overall increase in atmospheric CO_2 concentrations. While the emission of H_2S from landfills is typically minimal, it is odorous and prolonged exposure can lead to chronic health impacts. In order to tackle these issues, researchers at the University of Illinois at Chicago devised a novel biogeochemical cover (BGCC) that integrates biochar-amended soil (BAS) and basic oxygen furnace (BOF) steel slag. This cover was designed for concurrent removal of CH_4, CO_2, and H_2S gases [11, 12]. The addition of BAS helps mitigate CH_4 emissions, while BOF slag facilitates the carbonation and sulfidation processes to mitigate CO_2 and H_2S, respectively.

Several series of laboratory column experiments were carried out to mimic different configurations of BGCC profiles. These experiments showcased substantial promise in eliminating CH_4, CO_2, and H_2S gases under the conditions resembling those found in landfills. [11, 12]. However, the effectiveness of the BGCC has not yet been tested in the field. Therefore, a near-field scale tank setup of BGCC profile was established in laboratory-controlled conditions to assess the performance of BGCC system. The purpose of this research is to examine the dynamics of CH_4 oxidation within BAS layer in the BGCC system. The scope of research included: (1) developing near-field scale test setup of biogeochemical cover, (2) assessing CH_4 oxidation in biochar-amended soil (biocover) layer in BGCC with gas monitoring in biocover layer as a function of time, and (3) determining spatial variation in physico-chemical properties and CH_4 oxidation potential of biocover layer by collecting samples from the different spatial locations (at the same depth location). The comprehensive evaluation of CO_2 and H_2S capture by the slag layer was conducted; however, these details are not covered within the focus of this paper.

2 Materials and Methods

2.1 Materials

The materials used in BGCC profile comprised of soil, biochar, and BOF steel slag, geotextile fabric, and geocomposite drainage mat. The soil was collected from different locations of the intermediate cover of landfill situated in Zion, Illinois, whereas the BOF steel slag was procured from Indiana Harbor East (IHE), Indiana. The pinewood-derived biochar used as an organic amendment in biocover layer of the cover profile was in the form of pellets and was procured from Chip Energy Inc. (Goodfield, IL, USA). The properties of 10% (w/w) BAS, soil, biochar, and BOF slag are outlined in Table 1. The geotextile was sourced from EPI- The Liner Company in Traverse City, Michigan, while the geocomposite was obtained from SKAPS Industries in Georgia, USA.

Table 1 Properties of biogeochemical cover (BGCC) components used in near-field scale tank setup

Properties	ASTM method	BGCC				
		10% (w/w) BAS	Soil	Biochar	BOF slag	Topsoil
Specific gravity	D854	2.59	2.72	1.23	3.41	2.70
Organic content (%)	D2974	8.1	4.0	98.5	2.0	4.5
Grain size distribution						
Gravel (%)	D6913/6913 M	0.8	0	30.4	20	0
Sand (%)	D7928	41.4	37.9	69.3	73.4	38.4
Silt (%)		35.8	43.1	0.3	6.6	36.6
Clay (%)		22.0	19.0	0.0	0	25.0
USCS classification		CL	CL	SP	SW-SM	CL
Liquid limit	D4318	30	31	NP	NP	32
Plastic limit		19	17			18
Water holding capacity (%w/w)	D2980	54	58	43	25	56
Hydraulic conductivity (cm/s)	D5084/D2434	5.8×10^{-6}	–	3.4×10^{-3}	8.3×10^{-3}	1.84×10^{-7}
@ Dry density		@1.10		@0.5	@2.23	@1.15
pH (1:5)	D4972	8.4		–	12.8	8.7
Carbonate content (% $CaCO_3$)	D4373	14.6	14.6	3.5	2.35	15.2

Note BAS—biochar-amended soil, BOF slag-basic oxygen furnace slag

2.2 Near-Field Scale Tank Setup

A large, near-field scale square-shaped tank with a width of 0.5 m and a height of 1 m was fabricated to simulate near-field scale conditions (Fig. 1). The tank was made of stainless steel and was supported on a metal cart equipped with wheels to facilitate mobility. At the base of the tank, an opening was provided for the injection of synthetic LFG from the bottom. The flange with screw connections was provided at the top of the tank to support the placement of the top cap. The top cap, designed with a central opening, allowed the tank to be exposed to the atmosphere and facilitated the venting of surface emissions to the fume hood. Prior to introducing the synthetic LFG into the tank, it was routed through a water column to maintain the gas in humid state. Then, it passed through a flowmeter to control the flow and influx of the humidified

gas. Gas probes were located at different depths, and gas samples were collected and analyzed periodically. The gas probes located in BAS layer at 50 cm below the ground surface (bgs) and the measured gas concentration (CH_4, CO_2, and O_2), were selected for analyzing the effectiveness of BAS for CH_4 oxidation in this paper.

2.3 Preparation of Biogeochemical Cover (BGCC)

Figure 1 shows the BGCC profile created in the tank. The geocomposite layer (0.5 cm thick) was provided at the base of the tank to act as a gas distribution layer. The BGCC profile comprised a lower biocover layer, which consisted of a 45 cm thick BAS, responsible for CH_4 oxidation, a middle 30-cm-thick layer of BOF slag for sequestration of CO_2/H_2S and acting as drainage layer, and an upper topsoil vegetative soil layer of 15 cm thickness (Fig. 1). The BAS layer was filled in 5 cm intervals with gentle compaction.

Before placing the BAS mixture in the tank, it was modified to have a moisture content (MC) of 15% by weight. This specific MC was selected based on previous research that identified the ideal level of moisture needed for effective CH_4 oxidation [13]. The BAS was introduced into a tank with a bulk density of 1.21 g/cm^3 and an overall porosity of 60%. Over BAS layer, a 30 cm-thick layer of BOF slag that had been modified to include 10% (by weight) of moisture was applied in 5 cm lifts with comparable compaction efforts. The bulk density and the total porosity of the BOF slag inside the tank was 2.14 g/cm^3 and 44%, respectively. Lastly, a topsoil layer of 15 cm thick was placed above the BOF slag at a bulk density of 1.33 g/cm^3. This layer was modified to have a 15% MC. Each layer including BAS, BOF slag, and topsoil was separated by geotextile.

2.4 Biogeochemical Cover Testing Procedure

Humidified synthetic LFG was continuously injected from the bottom port of the tank for 304 days in five different phases (Phases 1–5), each with a different gas flow rate and composition. Additionally, 100 ml of deionized water was sprinkled over the tank every week to compensate for surface drying. During the Phase 1, a gas mixture of 1000 ppm CH_4 and 99.99% N_2 was introduced into the tank at an influx rate of around 0.1 g CH_4 m^{-2} day^{-1} for nearly 36 days to accustom the microbial population to tank conditions. On 36th day, the inlet gas composition was changed to synthetic LFG comprising a mixture of 50% CH_4 and 50% CO_2 at an influx rate of around 23.9 g CH_4 m^{-2} day^{-1} for the next 113 days under Phase 2. As a part of Phase 3, after 149th day, inlet gas composition was switched to 48.25% CH_4, 50% CO_2, and 1.75% H_2S to evaluate the effect of H_2S on CH_4 oxidation potential of biocover. The influx during this phase was maintained at approximately 25.5 g CH_4 m^{-2} day^{-1}for the next 74 days. After 222 days, the gas composition was changed back to 50%

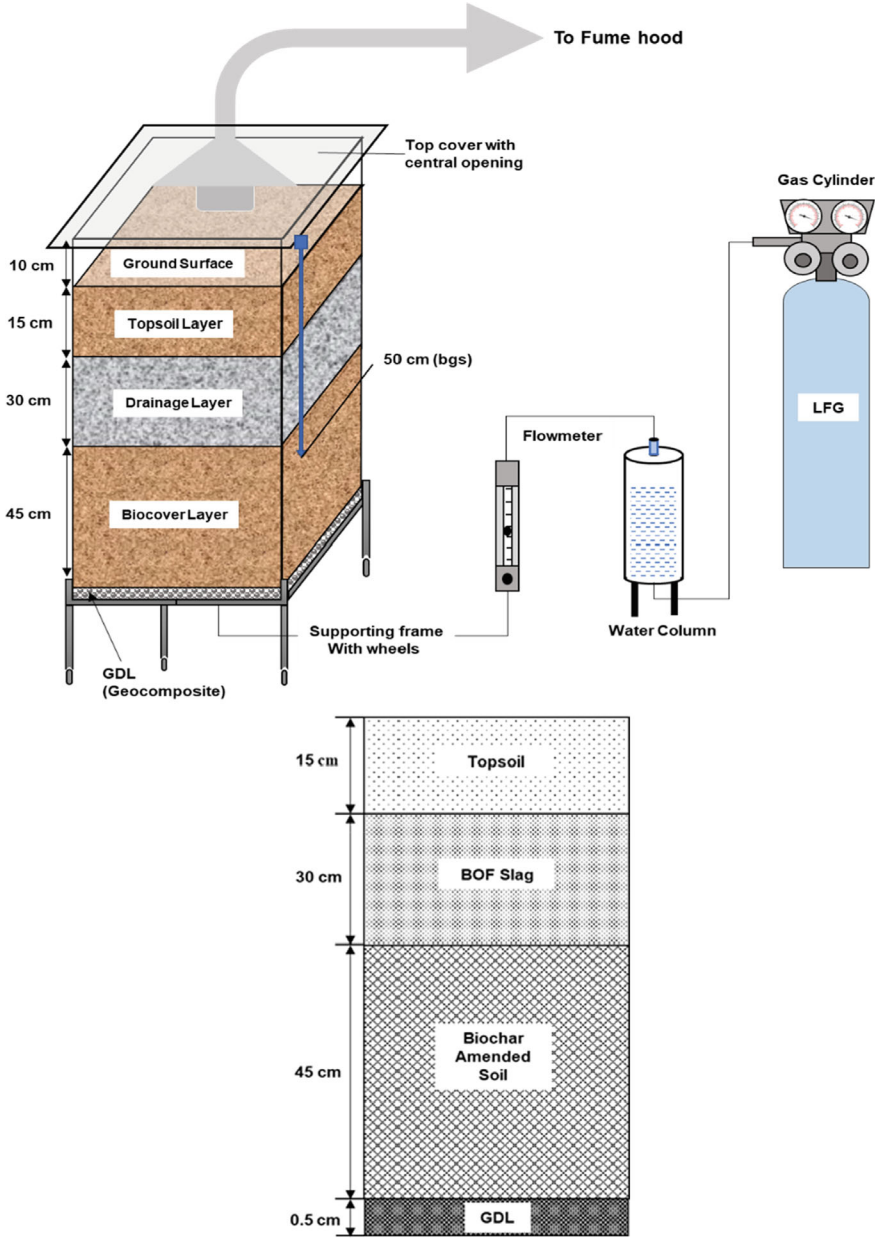

Fig. 1 Schematic of near-field scale tank setup and biogeochemical cover (BGCC) profile. *Note* GDL—gas distribution layer

CH_4 and 50% CO_2 during Phase 4. The gas was introduced at a higher flow rate, approximately double the rate used during Phase 2, with a flux rate of 57.5 g CH_4 m^{-2} day^{-1}. This alteration was made to assess the capability of microorganisms to oxidize CH_4 under these increased flow conditions. In Phase 5, the gas composition (50% CH_4 and 50% CO_2) and flux rate (25.3 g CH_4 m^{-2} day^{-1}) were restored back to their values like in Phase 2. This was done to study the resilience behavior of microbial communities to changing gas composition and flux. Each phase was operated until the gas concentration profiles at a depth remained stable. Gas samples were collected once a week using a syringe (1 mL) with a luer lock. Afterward, the collected gas samples were then examined using SRI 9300 gas chromatography equipped with flame ionization/flame protonation detectors and thermal conductivity detector to detect CH_4, CO_2, and O_2.

2.5 Tank Exhumation

The tank experiment was terminated following continuous flushing of synthetic LFG for a period of 304 days, employing various gas composition and flux rates. Subsequently, all materials were carefully extracted, sampled at different depths and spatial locations and saved for further analysis. The BAS samples collected at a depth of 50 cm (bgs) and various spatial locations and the monitoring data from the gas probes located at the same depth are selected for detailed analysis in this paper. This sampling allowed to investigate the spatial variations in the physico-chemical properties of BAS post-termination of the experiment. MC, organic content, and pH were assessed for all the collected samples. To account for spatial variations, the entire cross section was divided into 25 sampling locations, each measuring 10×10 cm^2, covering multiple locations.

Figure 2 shows the sampling locations and sample designations. Additionally, some of the extracted BAS samples were also subjected to batch testing as per the procedure outlined in Chetri et al. [9] to determine potential CH_4 oxidation rates. Approximately 10 g of the extracted samples were meticulously placed in 125 ml glass vials and tightly sealed with rubber septa and metal crimp caps. Following the sealing process, 20 ml of headspace air was extracted using a 100 ml syringe, and subsequently substituted with 20 ml of a gas mixture consisting of 50% CH_4 and 50% CO_2. The concentrations of CH_4 and CO_2 in the headspace were monitored diligently daily until the CH_4 concentration reached zero. The samples chosen for the batch testing corresponded to sampling locations: 5, 9, 13, 17, and 21.

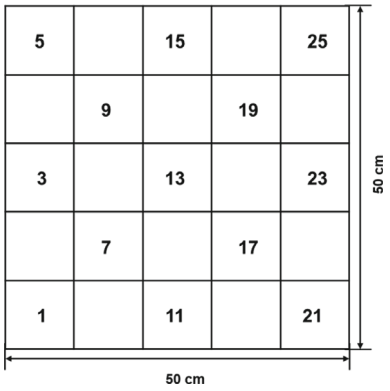

Fig. 2 Sampling locations within biochar-amended soil layer (at a depth of 50 cm (bgs))

3 Results and Discussion

3.1 Dynamics of Methane Oxidation

Figure 3a–c illustrates the gas concentrations of CH_4, CO_2, and O_2 in biocover layer relative to their corresponding inlet concentrations. The biocover demonstrated significant CH_4 removal, evident from the decreased CH_4 concentration near the top of the biocover during each phase (Fig. 3a). This observation indicates the significant microbial oxidation of CH_4 in the presence of O_2 into CO_2. Analyzing the average CH_4 concentrations in biocover layer during each phase, it was found that only 16.6% of the inlet CH_4 was detected in Phase 2, followed by 19.86% in Phase 3, 30.5% in Phase 5, and 64.85% in Phase 4. The average O_2 concentration measured at same depth in biocover layer exhibited a narrow range of variations (1.24–1.99%) across all phases, except for Phase 2, where the average concentration (3.35%) was detected, which was slightly higher compared to the other phases (Fig. 3c). This indicates a more amount of O_2 was consumed by microorganisms for CH_4 oxidation, resulting in increased CO_2 production in all phases relative to Phase 2, as depicted in Fig. 3b

Based on the average CH_4 concentrations detected in biocover during each phase relative to the inlet concentrations injected, it can be inferred that Phase 2, characterized by a gas composition of 50% CH_4 and 50% CO_2, and a flux rate of 23.9 g CH_4 m^{-2} day^{-1}, exhibited the highest CH_4 reduction relative to its respective inlet concentration. Conversely, the lower CH_4 reduction relative to inlet concentration was observed during Phase 4, where the inlet flux rate was doubled. The higher concentration of CH_4 observed during Phase 4 can be attributed to the limited time of contact between methanotrophs (CH_4-oxidizing bacteria) and CH_4. As a result, there is limited microbial oxidation of CH_4 during this phase, leading to a detection of higher CH_4 concentration. Even though there was a slight difference in the average CH_4 reduction in biocover layer between Phase 2 and Phase 3, this reduction could potentially be ascribed to several factors, one of which may include the inhibitory influence of H_2S gas during Phase 3, which had a gas composition of 48.25% CH_4,